Inorg. Chem. **2004**, *43*, 4300–4305

Influence of the [2.1.1]-(2,6)-Pyridinophane Macrocycle Ring Size Constraint on the Structure and Reactivity of Copper Complexes

A. N. Vedernikov, M. Pink, and K. G. Caulton*

Department of Chemistry and Molecular Structure Center, Indiana University, Bloomington, Indiana 47405

Received January 28, 2004

The macrocycle [2.1.1]-(2,6)-pyridinophane (L) binds to CuCl to give a monomeric molecule with tridentate binding of the ligand but in a distorted tetrahedral "3 + 1" geometry, where one nitrogen forms a longer (by 0.12 Å) bond to Cu. In dichloromethane solvent this pyridine donor undergoes facile site exchange with a second pyridine in the macrocycle, to give time-averaged mirror symmetry. Both experimental and density functional theory studies of the product of chloride abstraction, using $NaBAr^F_4$ in CH_2Cl_2, show that the Cu^+ binds in a trigonal pyramidal, not planar, arrangement in LCu^+. This illustrates the ability of macrocyclic ligand constraint to impose an electronically unfavorable geometry on 3-coordinate Cu(I). $LCuBAr^F_4$ and a triflate analogue $LCu^I(OTf)$ readily react with oxygen in dichloromethane to produce, in the latter case, a hydroxo-bridged dimer $[LCu^{II}(\mu\text{-}OH)]_2(OTf)_2$, of the intact (unoxidized) ligand L. Since the analogous LCuCl does not react as fast with O_2 in CH_2Cl_2, outer-sphere electron transfer is concluded to be ineffective for oxidation of cuprous ion here.

Introduction

The pyridinophane ligand **L** is a newly synthesized ligand designed to complement centrally connected tripodal ligands carrying three neutral nitrogen donors such as $HB(pz)_3^-$ and $HC(pz)_3$, the tris(pyrazolyl)borates and -methanes.[1] The design element of the [*n.m.p*]-pyridinophanes of special

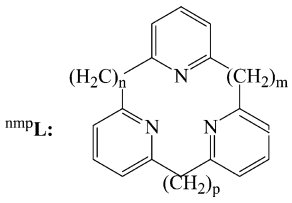

importance is the length of the linker elements $(CH_2)_q$, which governs the macrocycle size and thus controls the coordination geometry of the three pyridyl nitrogens around a single metal.[2] Thus, for smaller macrocyles, the metal cannot fit into the ^{211}**L** macrocycle (i.e. cannot become coplanar with all three N), and the geometry of the pyridinophane will be necessarily *facial* (i.e. all cis) on the metal. Even the free ^{211}**L** ligand itself does *not* have the nitrogen lone pairs coplanar or converging.[2,3] In some cases, the facial geometry will lead to *cis*-N−M−N angles highly distorted from those preferred by the metal, which in turn may make η^2-binding to the metal more favorable than η^3-binding. This is the case for divalent Pt in $LPtCH_3^+$,[4] $LPtH^+$,[5] and also in LMX_2 (M = Pd, Pt, X = Cl, CH_3),[2,3] and the pendant nitrogen can then play an active and stabilizing role in chemical reactivity.[6] It influences both reactant and product. In brief, it has been shown to form a bond to Pt^{IV}, after oxidation, and thus provide product stability (octahedral Pt^{IV}) for even the challenging cleavage of an alkane C−H bond. Because it is an intramolecular effect, it occurs *without* the entropy penalty involved with coordinating a truly free (i.e. solution phase) ligand to product. It can also accept a proton during the heterolytic cleavage of an arene C−H bond,[6] again providing some enthalpic benefit at minimal entropy cost. The resulting pendant pyridinium functionality can then hydrogen bond to the filled d_{z^2} orbital of a planar 4-coordinate Pt^{II} product,

* Author to whom correspondence should be addressed. E-mail: caulton@indiana.edu.

(1) Trofimenko, S. *Scorpionates: The Coordination Chemistry of Polypyrazolylborate ligands*; Imperial College Press: River Edge, NJ, 1999.
(2) Vedernikov, A. N.; Pink, M.; Caulton, K. G. *J. Org. Chem.* **2003**, *68*, 4806.
(3) Vedernikov, A. N.; Huffman, J. C.; Caulton, K. G. *Inorg. Chem.* **2002**, *41*, 6867.
(4) Vedernikov, A. N.; Huffman, J. C.; Caulton, K. G. *New J. Chem.* **2003**, *27*, 665−667.
(5) Vedernikov, A. N.; Caulton, K. G. *Angew. Chem., Int. Ed.* **2002**, *41*, 4102−4104.
(6) Vedernikov, A. N.; Caulton, K. G. *Chem. Commun.* **2003**, 358.

10.1021/ic049886o CCC: $27.50
Published on Web 05/25/2004

or it can participate in an intramolecular redox *equilibrium* via the hydrogen transfer illustrated in eq 1.[2] We have also

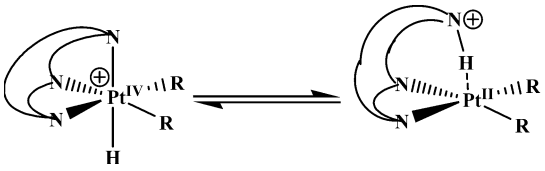

(1)

established[2] that such ligand constraints can impose metal complex reactant destabilization, which has the obvious effect of improving reaction thermodynamics (via enthalpy); this can be especially important in trying to cleave strong and poor donor bonds (e.g. alkane C−H) where we have shown computationally that CH_4 bond cleavage by a typical planar 4 coordinate Pt^{II} species is endergonic but reactant destabilization by progressive ring constraints by ^{nmp}**L** can lead to an exergonic methane oxidative addition reaction. Experimental determination of the structure of some four-coordinate $^{211}LMX_2$ species (M = Pd, Pt; X = Cl, CH_3) has actually revealed more: the nonbonded pyridine has an N/M distance (2.658 Å) short enough to reveal[3] a filled/filled repulsion between the pendant N lone pair and the filled d_{z^2} orbital. This has the result of increasing the reducing power of the species because, as in hydrazine and other diamines which also have filled/filled repulsion, the filled antibonding combination of the two lone pairs has a lower ionization potential than does either lone pair alone. This then traces the origin of generalized reactant destabilization to its orbital origin.[7] While the Bronsted basicity functionality has been demonstrated for other multidentate amine *or* imine ligands when they bind to a metal with less than their full complement of nitrogen lone pairs,[8−10] comparison of those examples to pyridinophane Bronsted basicity can begin to establish how ligand internal connectivity and consequent angular constraints influences the effectiveness of such behavior. This paper begins such comparisons.

We have more recently tried to evaluate the suitability of the ^{211}**L** macrocycle to dictate reactivity enhancement on other metals. This objective represents significant new "terrain" since it involves other preferred coordination geometries than the planar/octahedral pair relevant to our exploration of d^8/d^6 platinum chemistry. We are, moreover, interested in moving to the less expensive 3d metals, and these immediately encounter (1) the relative inapplicability of the 16/18 electron rule and (2) the frequent occurrence of one- and not two-electron redox changes. These are of course related characteristics but ones which were not true of our use of pyridinophane on platinum. Moreover, it would appear that some alkane C−H cleavage reactions by metalloproteins can occur without formation of any metal−carbon bond: the classic oxidative addition (eq 2) or even electrophilic cleavage reactions (eq 3) are not relevant.

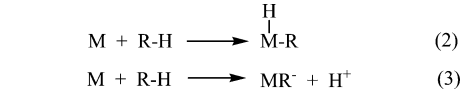

(2)

(3)

It is with an eye to exploring reactivity *different* from the reported Pt chemistry that we selected copper for testing of the macrocyclic constraint idea. This has led to the recent demonstration that copper complexes of [2.1.1]-2,6 pyridinophane catalyze rapid olefin aziridination.[11] They also catalyze oxidation of *saturated* hydrocarbons to olefins by $PhINSO_2$(tolyl) a reaction in which nitrogen receives the hydrogens removed in oxidizing alkane to olefin.[12] This report examines the structural outcome of conflicting steric and electronic preferences when the [2.1.1]-(2,6)-pyridinophane, **L**, is bound to CuCl where Cu^I would normally prefer tetrahedral geometry. The origin of distortions is analyzed both by comparison to the structure of an *acyclic* analogue of the pyridinophane bound to CuCl[13] and also by computational experiments where structures of systematically modified LCu^+ species are determined by geometry optimization using density functional theory (DFT[14] (PBE[15])). Reactivity of the LCu^I fragment toward dioxygen is also reported and shows the oxidation to occur at the metal but apparently only by electron transfer in an inner-sphere process which depends on O_2 first coordinating to Cu(I).

This study of the geometric distortions imposed by this pyridinophane macrocycle on Cu(I) and even Cu(II) therefore has enhanced importance in the exploitation of the macrocycle constraint idea.

Results and Discussion

LCuCl. Synthesis, Structure, and Solution NMR Behavior. The complex was synthesized by reaction of **L** with CuCl in benzene under anaerobic conditions. The molecule crystallizes (Figure 1) with no rigorous symmetry in a polar space group as a molecular species (Tables 1 and 2). In the LCuCl species, four coordinate Cu(I) is distorted from tetrahedral symmetry in a way which makes the pyridine rings involving N1 and N2 equivalent (by angles Cl−Cu−N and by their Cu−N distances) and N3 distinct (longer Cu−N distance by 0.12 Å and a smaller Cl−Cu−N angle, by over 14°). All of these distortions can be ascribed to the N2 pyridine ring not being able to direct *both ortho* CH_2 groups simultaneously in a way that will accommodate the N1 and N3 pyridine rings, and apparently it is the ring with the longer, more flexible CH_2CH_2 linker that is left to "suffer." The largest N−Cu−N angle involves the CH_2CH_2 linker (and thus a seven-membered $NCuNC_4$ ring).

An excellent comparison compound is the CuCl complex of the nonmacrocyclic tpdm ligand, which shows that the greater ligand flexibility/adaptability permits a larger

(7) Canty, A. J.; van Koten, G. *Acc. Chem. Res.* **1995**, *28*, 406.
(8) Jenkins, H. A.; Klempner, M. J.; Prokopchuk, E. M.; Puddephatt, R. J. *Inorg. Chim. Acta* **2003**, 72.
(9) Prokopchuk, E. M. P., R. J. *Organometallics* **2003**, *22*, 787.
(10) Puddephatt, R. J. *Coord. Chem. Rev.* **2001**, 157 and references therein.
(11) Vedernikov, A. N.; Caulton, K. G. *Org. Lett.* **2003**, *5*, 2591.
(12) Vedernikov, A. N.; Caulton, K. G. *Chem. Commun.* **2004**, 162.
(13) Vedernikov, A. N.; Huffman, J. C.; Caulton, K. G. *Inorg. Chem.* **2002**, *41*, 6244−6248.
(14) Parr, R. G.; Yang, W. *Density-functional theory of atoms and molecules*; Oxford University Press: Oxford, U.K., 1989.
(15) Perdew, J. P.; Burke, K.; Ernzerhof, M. *Phys. Rev. Lett.* **1996**, *77*, 3865.
(16) Que, L.; Tolman, W. B. *Angew. Chem., Int. Ed.* **2002**, *41*, 1114.

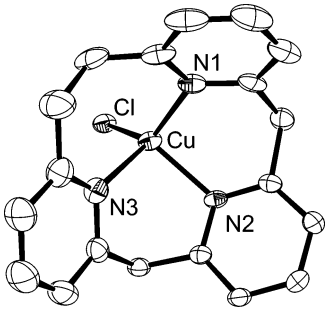

Figure 1. ORTEP drawing of LCuCl, omitting hydrogen atoms and showing selected atom labeling (50% probability level).

Table 1. Crystal Data and Structure Refinement for LCuCl and $[LCu(\mu\text{-}OH)]_2(OTf)_2$

	LCuCl	$[LCu(\mu\text{-}OH)]_2(OTf)_2$
empirical formula	$C_{19.33}H_{17.67}Cl_{1.67}CuN_3$	$C_{41}H_{38}Cl_2Cu_2F_6N_6O_8S_2$
fw	414.65	1118.87
cryst color, shape, size (mm^3)	yellow needle, 0.40 × 0.10 × 0.10	blue plate, 0.12 × 0.10 × 0.03
temp (K)	136(2)	113(2)
wavelength (Å)	0.710 73	0.710 73
cryst system, space group	hexagonal, $P6_1$	triclinic, $P\bar{1}$
unit cell dimens (Å, deg)	$a = 21.0593(16)$ $b = 21.0593$ $c = 7.5642(6)$ $\alpha = 90$ $\beta = 90$ $\gamma = 120$	$a = 9.9327(9)$ $b = 10.6687(10)$ $c = 11.3605(10)$ $\alpha = 83.677(2)$ $\beta = 69.113(2)$ $\gamma = 74.624(2)$
V ($Å^3$)	2905.2(3)	1084.33(17)
Z	6	1
d(calcd) (Mg/mm^3)	1.422	1.713
abs coeff (mm^{-1})	1.364	1.288
final R indices [$I > 2\sigma(I)$]	R1 = 0.0350, wR2 = 0.0811[a,b]	R1 = 0.0536, wR2 = 0.1264[a,b]

[a] $R1 = \sum(|F_o| - |F_c|)/\sum|F_o|$. [b] $wR2 = [\sum[w(F_o^2 - F_c^2)^2]/\sum[w(F_o^2)^2]]^{1/2}$.

Table 2. Selected Bond Lengths (Å) and Angles (deg) for LCuCl

Cu1−N1	2.052(3)	Cu1−N3	2.190(3)
Cu1−N2	2.069(2)	Cu1−Cl1	2.2305(8)
N1−Cu1−N2	90.30(10)	N1−Cu1−Cl1	129.28(8)
N1−Cu1−N3	99.65(11)	N2−Cu1−Cl1	126.53(7)
N2−Cu1−N3	90.32(10)	N3−Cu1−Cl1	111.96(8)

$\angle N^t-Cu-N^t$, more equal Cu−N distances, and thus approximate mirror symmetry.[13]

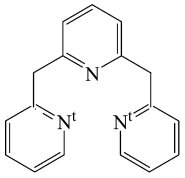

tpdm

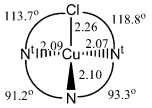

∠ Cl-Cu-N = 124.2°
∠ N^t-Cu-$N^{t\prime}$ = 111.5°

Figure 2a,b illustrates the following:

(a) A "3 + 1" designation of the coordination geometry is appropriate with the long Cu−N3 distance symbolized by "1".

(b) Cu is close to coplanar with the "3" ligands designated above, Cl, N2, and N1.

(c) The more weakly bound py (N3) is displaced angularly (toward N2 and thus off the idealized mirror plane relating N2 and N1) by the longer link, $(CH_2)_2$.

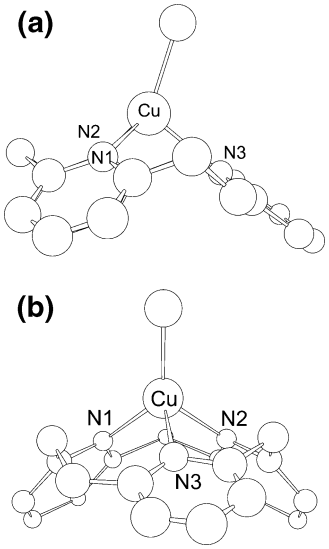

Figure 2. Two views of the experimentally determined structure, (a) viewing the ClCuN2N1 plane edge-on and (b) rotated 90° about the Cu−Cl vector from (a).

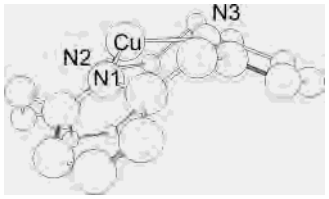

Figure 3. Calculated (DFT) geometry-optimized structure of the three-coordinate cation LCu^+: Cu−N3, 1.975 Å; Cu−N2, 1.940 Å; Cu−N1, 1.927 Å; N3−Cu−N2, 104.7°; N1−Cu−N3, 102.9°; N2−Cu−N1, 122.7°.

(d) The angular distortion from tetrahedral (or 3-fold) symmetry involves Cl bending toward N3, which is the weakly bound nitrogen.

All parameters of the DFT-calculated structure of LCuCl match closely (≤2% for bond lengths, ≤2° for bond angles) those found by X-ray diffraction in the solid state.

Despite the lack of mirror symmetry in the solid state caused by the staggered gauche conformation of the macrocycle ethylene bridge, LCuCl behaves as a mirror symmetric species on the ^1H NMR time scale in CD_2Cl_2 solution at 22 °C. The macrocycle exhibits two doublets for the methylene bridges at 4.11 and 4.71 ppm, three doublets of equal intensity for the *meta*-protons of the macrocycle pyridine residues, and two triplets of corresponding *para*-protons at 7.50 and 7.60 in 2:1 ratio. The spectral pattern does not change at −45 °C. The ^{13}C NMR spectrum is also consistent with this conclusion about the symmetry of LCuCl in solution.

Three-Coordinate Nonplanar LCu^+? a. Computed Geometry. To establish the Cu^I binding preference of L in the *absence* of a fourth ligand, the structure of LCu^+ was also optimized by a DFT (PBE) method.[14,15] The result (Figure 3) shows clearly that Cu^I cannot fit into the N_3 plane, and so the trigonal planar geometry found for a three-coordinate d^{10} metal must be distorted. The N−Cu−N angles are all larger than in LCuCl, and all Cu−N distances are shorter, all consistent with Cu moving closer to the N_3 plane. As in LCuCl, the N−Cu−N distance involving the longer

$-CH_2CH_2-$ linker is larger, and there is enough flexibility that the hydrogens in this linker can adopt a staggered conformation. The Cu/N distances in LCu^+, although they are distinctly different (by 0.05 Å), do not show as great a variation as those in LCuCl (0.137 Å).

b. Experiment. The formally three coordinated cation LCu^+ could be generated by abstraction of chloride ligand by $NaBAr^F{}_4$ ($BAr^F{}_4$ = tetrakis[3,5-bis(trifluoromethyl)-phenyl]borate) in the low coordinating solvent dichloromethane. Stirring a slight excess of this reagent with a dichloromethane solution of LCuCl at room temperature leads to its fast dissolution and then the appearance of another precipitate. The resulting light-yellow solution exhibited ^1H and ^{13}C NMR spectra consistent with a formula for the soluble product as $LCuBAr^F{}_4$, containing a cation of mirror symmetry at both 22 and −45 °C. The signals of its methylene bridges appeared as a broadened AB quartet while protons of the ethylene bridge showed two broad singlets at 22 °C, which resolved at −45 °C into multiplets. At both temperatures the aromatic signals showed three sharp doublets and two triplets. Thus, in accordance with DFT calculations, the resulting three-coordinated copper complex, which might weakly coordinate dichloromethane, remains pyramidal and does not display any evidence of the copper atom to migrate *through* the macrocycle hole, which would lead to coalescence of signals of the $(CH_2)_n$ bridges.

Reactivity under Oxidizing Conditions. a. General Comments. The observed[11] copper-catalyzed olefin aziridination must begin by coordination of PhINTs, to Cu, and perhaps even loss of PhI to leave behind a copper/NTs species which contains oxidized copper (Cu^{III} or Cu^{II}); this conclusion follows because there is no detectable olefin coordination to the L/Cu species. Similarly, spectroscopic and ESI-mass spectrometric observation[11] of the L/Cu + alkane + PhINTs reacting system has shown the presence of NTs complexed to one, and also two copper centers, and with oxidation states higher than +1. DFT calculations show[11] that several Cu(II) species seen by ESI-MS and detected by ^1H NMR spectroscopy are at energies low enough to make them candidates for participants in the oxidation of alkane to olefin.[12] It thus becomes important to begin to define the reaction chemistry of LCuX with aprotic oxidants in non-Bronsted acidic medium. This takes on enhanced importance because these two examples of catalysis by ^{211}**L**Cu catalyst precursors both show evidence of limited catalyst lifetime, suggesting (oxidative) catalyst degradation. We therefore studied the reactivity of LCuX species toward O_2, an oxidant for which there is a vast resource of literature precedent.[16] Only studies in the most recent 10 years have used low-temperature conditions to detect primary products (ligated CuO_2^+ and $Cu_2O_2^{2+}$, the latter as redox isomers) and show the complexity of these reactions that ultimately produce secondary products which frequently involve (intramolecular) attack on ligand C−H bonds.

b. Reactions of LCuX (X = $BAr^F{}_4$, OTf, Cl) with Oxygen. Reactivity of complexes of general formula LCuX toward oxygen may provide important information about the ability of this new species to be oxidized by one electron (forming Cu^{II}) or two (forming Cu^{III}), as well as about the ability of the pyridinophane macrocycle attached to the metal to resist oxidative degradation. The latter might occur first at the thermodynamically most vulnerable benzylic carbons linking three pyridine rings together.[17] However, there are also many examples of pendant aryl "hydroxylation."[16] The effect, if any, of the ability of X to remain coordinated to copper on this reactivity can shed some light on the nature of plausible reaction intermediates. Indeed, three copper(I) pyridinophane complexes studied here (X = $BAr^F{}_4$, OTf, Cl) showed significantly different reactivities.

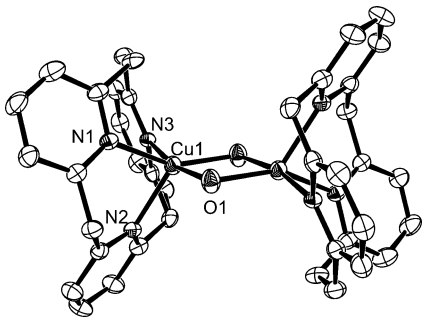

Figure 4. ORTEP drawing of the centrosymmetric dication in $L_2Cu_2(\mu\text{-}OH)_2(OTf)_2$, omitting hydrogen atoms and showing selected atom labeling (50% probability level).

Table 3. Selected Bond Lengths (Å) and Angles (deg) in the Ion $[LCu(\mu\text{-}OH)]_2^{2+}$

Cu1−O1	1.930(5)	Cu1−N3	2.111(4)
Cu1−O1$^{\#1}$	1.962(5)	Cu1−N2	2.135(4)
Cu1−N1	2.108(3)	Cu1−Cu1$^{\#1}$	3.0013(11)
O1−Cu1−O1$^{\#1}$	79.1(2)	O1−Cu1−N2	123.86(18)
O1−Cu1−N1	90.3(2)	O1$^{\#1}$−Cu1−N2	103.68(18)
O1$^{\#1}$−Cu1−N1	167.5(2)	N1−Cu1−N2	87.66(16)
O1−Cu1−N3	150.09(19)	N3−Cu1−N2	85.90(14)
O1$^{\#1}$−Cu1−N3	91.75(18)	Cu1−O1−Cu1$^{\#1}$	100.9(2)
N1−Cu1−N3	94.37(16)		

i. $BAr^F{}_4$ Salt. When a solution of $LCuBAr^F{}_4$ in dichloromethane was exposed at −90 °C to oxygen (2:1 mole ratio), an immediate dark brown color appeared which turned to green after the sample was allowed to warm to room temperature. Removal of solvent produced a dark green oil, which resisted attempts at crystallization.

ii. $CF_3SO_3^-$ Salt. A similar experiment performed with LCu(OTf) showed similar but much slower reactivity. The reaction mixture, warmed to room temperature, changed its color from dark brown to yellow-green. All LCu(OTf) was consumed in 30 min as evidenced by ^1H NMR. Standing 12 h at 22 °C lead to formation of small bluish-green crystals of $[(\eta^3\text{-L})Cu(\mu\text{-OH})]_2(OTf)_2$ suitable for X-ray structure determination in 40% isolated yield.

The product is a dimer, centrosymmetric in the unit cell, with two Cu(II) bridged by two hydroxides (Tables 1 and 3 and Figure 4). Each hydroxide proton[18] is hydrogen bonded to a triflate oxygen with an O/O distance of 2.58 Å. The Cu−OH distances, 1.930(5) and 1.962(5) Å, are too long to belong to an oxo ligand on Cu(III) (typically 1.80 Å[16,19])

(17) Spodine, E.; Manzur, J.; Garland, M. T.; Fackler, J. P., Jr.; Staples, R. J.; Trzcinska-Bancroft, B. *Inorg. Chim. Acta* **1993**, *203*, 73.
(18) The origin of the hydroxyl proton was not determined.

and fall in the range typical for $Cu^{II}_2(\mu\text{-}OH)_2^{2+}$ units. The near-3-fold symmetry of the pyridinophane leaves all three Cu−N distances nearly identical (2.108(3)−2.135(4) Å); the N−Cu−Cu′ angles fall in a narrow range (120.86(10)−129.86(15)°), which indicates that "square pyramidal" is an imperfect description of the five coordinate polyhedron. As seen in Figure 4, the closest approach to square pyramidal geometry would have N2 as the apical group. The "bite" angles of the pyridinophane (N−Cu−N) range from 85.90(14) to 94.37(16)°, which is generally 5° smaller than in LCuCl.

iii. Cl Complex. Finally, a dichloromethane solution of the *chloro* complex exposed to oxygen reacted very slowly even at 22 °C so that its transformation was not complete even in 1 month to produce an amorphous green precipitate. Thus, stronger coordination of X to the metal in (formally) cationic LCu^+ inhibits oxidation of copper(I) in these pyridinophane complexes. These facts imply that precoordination of oxygen to copper is necessary for redox reaction and outer-sphere electron transfer is not involved. The observed color changes, in particular, the initial brown color and ultimate formation of $[LCu(\mu\text{-}OH)]_2^{2+}$ species, are similar to those previously observed for *tacn* complexes[19] and indicate possible formation of an intermediate like $[LCu^{III}(\mu\text{-}O)]_2^{2+}$. Finally, isolation and characterization of $[LCu(\mu\text{-}OH)]_2(OTf)_2$, whose benzylic protons are intact, shows some resistance of the macrocycle toward oxidation.

Conclusions

Systematic modification of the nucleophilicity of the anion X in LCuX has revealed that chloride, the least likely ligand to dissociate to free X^- in CH_2Cl_2 solvent, is in fact quite protected against reaction with O_2. This suggests that O_2 oxidizes these Cu(I) species only by an inner-sphere mechanism, via coordinated O_2, and not effectively by an outer-sphere mechanism. Clearly this demonstration hinges on a coordination number of 4 being retained, so it indicates not only retention of the Cu−Cl bond but also the persistence of η^3 binding of the pyridinophane, despite the observed variation of Cu−N distances in LCuCl. This suggests that the impact of the macrocycle here is not so much in reactant destabilization but that destabilization occurs instead when copper reaches higher oxidation states. The structure of $[LCu^{II}(OH)]_2^{2+}$ shows that the macrocycle nicely accommodates the 90° ± 4° angles of a facial ligand geometry, so it is perhaps at Cu^{III} (d^8 planar) that the biggest impact of a macrocycle constraint should be sought in the future. When the ligand is dissociation prone or dissociated ($CF_3SO_3^-$ and BAr^F_4, respectively), then the fact that copper is in an unusual *pyramidal* geometry for coordination number 3 (Figure 3) will, however, enhance the enthalpy of its reactions. Note also the flexibility of the 2.1.1-pyridinophane, in that ∠N−Cu−N varies from 90° (in $(LCuOH)_2^{2+}$) to 123° (in LCu^+).

Experimental Section

General Methods. All manipulations were carried out under purified argon using standard Schlenk and glovebox techniques. Solvents were dried and distilled by following standard protocols and stored in gastight bulbs under argon. All reagents for which a synthesis is not given are commercially available from Aldrich or Pressure Chemicals and were used as received without further purification. All NMR solvents were dried, vacuum-transferred, and stored in an argon-filled glovebox. [2.1.1]-(2,6)-pyridinophane was synthesized according to the published procedure.[3] ^1H and ^{13}C NMR spectra were recorded on Inova 700 spectrometer (^1H 400 MHz; ^{13}C 100.62 MHz). ^1H and ^{13}C NMR chemical shifts are reported in ppm and referenced to residual solvent resonance peaks.

Computational Details. Theoretical calculations in this work have been performed using the density functional theory (DFT) method,[14] specifically functional PBE,[15] implemented in an original program package "Priroda".[20] The applicability of the PBE functional for calculation of geometry of Cu(I) and Cu(II) complexes as well as its comparison with B3LYP was described before.[21] In PBE calculations, relativistic Stevens−Basch−Krauss (SBK) effective core potentials (ECP)[22−24] optimized for DFT calculations have been used. The basis set was 311-split for main group elements with one additional polarization p-function for hydrogen and an additional two polarization d-functions for elements of higher periods. Full geometry optimization has been performed without constraints on symmetry. For all species under investigation frequency analysis has been carried out. All minima have been checked for the absence of imaginary frequencies.

LCuCl, $C_{19}H_{17}ClN_3Cu$. To a dry flask containing a magnetic stirring bar was added, in a glovebox, CuCl (99 mg, 1.0 mmol) and 20.0 mL of dry benzene. To the stirred mixture was added [2.1.1]-(2,6)-pyridinophane (287 mg, 1.0 mmol) dissolved in 5.0 mL of benzene. Stirring was continued at room temperature for 5 h. The orange precipitate formed was filtered off, washed twice with 1.0 mL portions of benzene, and dried. Yield: 320 g (80%). Long yellow needles suitable for X-ray structural determination have been obtained by slow evaporation of a saturated solution LCuCl in a dichloromethane−benzene mixture.

^1H NMR (CD_2Cl_2, 22 °C): 3.25 (m, 2H, C_2H_4), 4.11 (d, J = 13.0 Hz, 2H, CH_2), 4.38 (m, 2H, C_2H_4), 4.71 (d, J = 13.0 Hz, 2H, CH_2), 7.10 (d, J = 8.0 Hz, 2H, *meta*-CH), 7.12 (d, J = 7.8 Hz, 2H, *meta*-CH), 7.25 (d, J = 7.8 Hz, 2H, *meta*-CH), 7.50 (d, J = 7.8 Hz, 2H, *para*-CH), 7.60 (d, J = 7.8 Hz, 1H, *para*-CH).

^{13}C NMR (CD_2Cl_2, −45 °C): 35.91 (CH_2), 46.54 (C_2H_4), 122.03, 122.26, 123.05 (*meta*-C, py), 137.25, 137.87 (*para*-C, py), 155.02, 155.51, 159.70 (*ortho*-C, py).

Reactions of LCuCl with $NaBAr^F_4$. In an argon-filled glovebox a Teflon-capped NMR Young tube was charged with 7.7 mg (20 μmol) of LCuCl, 18 mg (>20 μmol) of $NaBAr^F_4$, and 0.6 mL of CD_2Cl_2. The tube was closed, removed from the glovebox, and put into a rotating clamp to allow constant tumbling of the reaction mixture. In few minutes large chunks of $NaBAr^F_4$ dissolved, a new fine precipitate appeared, and the liquid color turned light-yellow. According to NMR data, all starting complex was consumed suggesting that the yield of $LCuBAr^F_4$ is almost quantitative.

^1H NMR (CD_2Cl_2, −45 °C): 3.32 (m, 2H, C_2H_4), 3.91 (m, 2H, C_2H_4), 4.16 (d, J = 13.8 Hz, 2H, CH_2), 4.24 (d, J = 13.8 Hz, 2H, CH_2), 7.17 (d, J = 7.8 Hz, 2H, *meta*-CH), 7.22 (d, J = 7.8 Hz, 2H, *meta*-CH), 7.32 (d, J = 7.8 Hz, 2H, *meta*-CH), 7.52 (br s, 4H,

(19) Aboelella, N. W.; Lewis, E. A.; Reynolds, A. M.; Brennessel, W. W.; Cramer, C. J.; Tolman, W. B. *J. Am. Chem. Soc.* **2002**, *124*, 10660.
(20) Ustynyuk, Y. A.; Ustynyuk, L. Y.; Laikov, D. N.; Lunin, V. V. *J. Organomet. Chem.* **2000**, *597*, 182.
(21) Vedernikov, A. N.; Wu, P.; Huffman, J. C.; Caulton, K. G. *Inorg. Chim. Acta* **2002**, *330*, 103.
(22) Cundari, T. R.; Stevens, W. J. *J. Chem. Phys.* **1993**, *98*, 5555.
(23) Stevens, W. J.; Basch, H.; Krauss, M. *J. Chem. Phys.* **1984**, *81*, 6026.
(24) Stevens, W. J.; Basch, H.; Krauss, M.; Jasien, P. *Can. J. Chem.* **1992**, *70*, 612.

para-CH, BAr^F_4), 7.57 (d, $J = 7.8$ Hz, 2H, *para*-CH), 7.66 (d, $J = 7.8$ Hz, 1H, *para*-CH), 7.71 (br s, 8H, *ortho*-CH, BAr^F_4).

^{13}C NMR (CD_2Cl_2, −45 °C): 35.97 (CH_2), 46.55 (C_2H_4), 117.73 (m, *para*-C, BAr^F_4), 123.02, 123.28, 123.97 (*meta*-C, py), 124.66 (quart, $^1J_{C-F} = 272.7$ Hz, CF_3, BAr^F_4), 128.88 (quart, $^2J_{C-F} = 31.7$ Hz, *meta*-C, BAr^F_4), 134.89 (br s, *ortho*-C, BAr^F_4), 138.89, 139.63 (*para*-C, py), 155.12, 155.73, 159.64 (*ortho*-C, py), 161.92 (quart, $^1J_{B-C} = 50$ Hz, B−C, BAr^F_4).

LCu(OTf), $C_{20}H_{17}F_3N_3SO_3Cu$. In a glovebox, to a dry flask containing a magnetic stirring bar were added CuOTf·0.5(PhMe) (258 mg, 1.0 mmol) and 20.0 mL of dry benzene. To the stirred mixture, [2.1.1]-(2,6)-pyridinophane (287 mg, 1.0 mmol) dissolved in 5.0 mL of benzene was added. Stirring was continued at room temperature for 5 h. The light yellowish-green precipitate formed was filtered off, washed twice with 1.0 mL portions of benzene, and dried. Yield: 450 g (90%).

Signals of LCu(OTf) in its ^1H NMR spectrum are broad at room temperature and become more narrow at −30 °C.

^1H NMR (CD_2Cl_2, −30 °C): 3.27 (m, 2H, C_2H_4), 4.11 (m, 2H, C_2H_4), 4.12 (d, $J = 13.0$ Hz, 2H, CH_2), 4.47 (d, $J = 13.0$ Hz, 2H, CH_2), 7.14 (d, $J = 7.8$ Hz, 2H, *meta*-CH), 7.17 (d, $J = 7.8$ Hz, 2H, *meta*-CH), 7.28 (d, $J = 7.8$ Hz, 2H, *meta*-CH), 7.54 (d, $J = 7.7$ Hz, 2H, *para*-CH), 7.62 (d, $J = 7.8$ Hz, 1H, *para*-CH).

^{13}C NMR (CD_2Cl_2, −30 °C): 35.90 (CH_2), 46.64 (C_2H_4), 122.43, 122.61, 123.42 (*meta*-C, py), 128.44 (CF_3), 137.68, 138.30 (*para*-C, py), 155.21, 155.64, 159.33 (*ortho*-C, py).

Reactions of LCuX (X = BAr^F_4, OTf, Cl) with O_2. In an argon-filled glovebox, a Teflon-capped NMR Young tube was charged with 40 μmol of corresponding LCuX dissolved in CD_2Cl_2 (1 mL, X = BAr^F_4; 1.5 mL, X = Cl; 2.0 mL, X = OTf). The tube was closed, removed from the glovebox, and cooled to −90 °C in an acetone bath. Argon was removed under vacuum, and the tube was filled with air (2.5 mL at 1 atm and 25 °C; 20 μmol of O_2).

Case a. In the case of X = BAr^F_4 a dark-brown color developed immediately; the change of color was slower in the case of X = OTf; no color changes was observed in the case of X = Cl. The tube was allowed to warm to 22 °C; the color turned green (X = BAr^F_4) or yellow-green (X = OTf). According to NMR data, the conversion of the starting complex was complete (X = BAr^F_4) in less than 10 or 30 (X = OTf) min. Removal of solvent afforded green noncrystallizable oil (X = BAr^F_4).

Case b. In the case of X = OTf, after 12 h, small bluish-green crystals of $[(\eta^3\text{-L})Cu(\mu\text{-OH})]_2(OTf)_2$ suitable for X-ray diffraction were collected and washed with a few drops of dichloromethane. Yield: 7.5 mg (40%). The ^1H NMR spectrum of the product exhibited broad but distinct signals of $[(\eta^3\text{-L})Cu(\mu\text{-OH})]_2(OTf)_2$.

^1H NMR (CD_2Cl_2, 22 °C): −0.52 (br s, 2H, CH_2), 1.39 (br s, 2H, CH_2), 3.03−3.49 (m, 2H, C_2H_4), 3.70−4.17 (m, 2H, C_2H_4), 9.55 (br s, 2H, *para*-CH), 10.15 (br s, 1H, *para*-CH), 13.99 (br s, 2H, *meta*-CH), 16.61 (br s, 2H, *meta*-CH), 17.34 (br s, 2H, *meta*-CH).

Case c. Oxidation of LCuCl was not complete (50% conversion) even in 1 month. A small amount of amorphous bluish-green precipitate of unknown composition had then formed on the bottom of the vessel.

X-ray Diffraction Structure Determination of [LCuCl·0.333CH_2Cl_2]. A yellow crystal (approximate dimensions 0.40 × 0.10 × 0.10 mm^3) was placed onto the tip of a 0.1 mm diameter glass capillary and mounted on a SMART6000 (Bruker) at 136 K. The data collection was carried out using Mo Kα radiation (graphite monochromator) with a frame time of 30 s and a detector distance of 5.1 cm. Three major sections of frames were collected with 0.30° steps in ω at three different ϕ settings and a detector position of −43° in 2θ. An additional set of 50 frames was collected to model decay. Data to a resolution of 0.77 Å were considered in the reduction. Final cell constants were calculated from the *xyz* centroids of 6999 strong reflections from the actual data collection after integration (SAINT)[25] The intensity data were corrected for absorption (SADABS).[26] The space group $P6_1$ was determined on the basis of intensity statistics and systematic absences. A direct-methods solution (SIR-92[27]) was calculated which provided most non-hydrogen atoms from the *E*-map. Full-matrix least-squares/difference Fourier cycles were performed which located the remaining non-hydrogen atoms (SHELXL-97[28]). All non-hydrogen atoms were refined with anisotropic displacement parameters except for the atoms belonging to the disordered solvent. The hydrogen atoms were placed in ideal positions and refined as riding atoms with relative isotropic displacement parameters. The remaining electron density is located in the solvent channel and in the vicinity of the copper and chlorine atoms of the complex.

X-ray Diffraction Structure Determination of $[L_2Cu_2(OH)_2(O_3SCF_3)_2\cdot CH_2Cl_2]$. A blue crystal (approximate dimensions 0.12 × 0.10 × 0.03 mm^3) was placed onto the tip of a 0.1 mm diameter glass capillary and mounted on a SMART6000 (Bruker) at 113(2) K. Data collection, solution, and refinement were generally as discussed above. A frame time of 80 s was used. Data to a resolution of 0.84 Å were considered in the reduction, and the intensity data were corrected for absorption (SADABS).[26]

There is a disorder of the pyridine ring that is attached to two different bridges, CH_2 and C_2H_4; it involves interchange of the CH_2 and C_2H_4 groups and consequent displacement of the pyridine ring (occupancy ratio 71:29). There is likewise a disorder of the hydroxide to a second position (68:32 occupancy). Disordered alternatives are labeled with a suffix "D". Given the close approach of these $Cu_2(\mu\text{-O})$ oxygens to triflate oxygens, there is no doubt that there are protons on the bridging atoms causing the short contact.

Acknowledgment. This work was supported by the DOE. A.N.V. is on leave from the Chemical Faculty, Kazan State University, Kazan, Russia. This work has been made possible in part due to support from the Russian Foundation for Basic Research (Grant No. 01.03.32692).

Supporting Information Available: Full crystallographic details (CIF and pdf files). This material is available free of charge via the Internet at http://pubs.acs.org.

IC049886O

(25) Bruker Analytical X-ray Systems, Madison, WI.
(26) Blessing, R. *Acta Crystallogr.* **1995**, *A51*, 33.
(27) SIR-92: Altomare, A.; Cascarno, G.; Giacovazzo, C.; Gualardi, A. *J. Appl. Crystallogr.* **1993**, *26*, 343.
(28) Bruker Analytical Systems, Madison, WI.